

www.acsnano.org

Probing the Mechanisms of Strong Fluorescence Enhancement in Plasmonic Nanogaps with Sub-nanometer Precision

Boxiang Song, Zhihao Jiang, Zerui Liu, Yunxiang Wang, Fanxin Liu, Stephen B. Cronin, Hao Yang, Deming Meng, Buyun Chen, Pan Hu, Adam M. Schwartzberg, Stefano Cabrini, Stephan Haas, and Wei Wu*



Cite This: https://dx.doi.org/10.1021/acsnano.0c01973



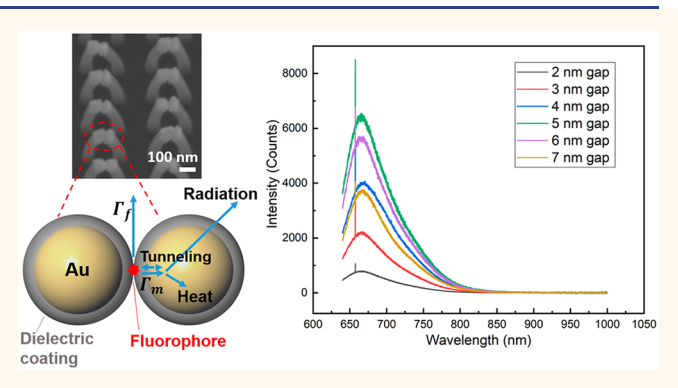
ACCESS

III Metrics & More

Article Recommendations

s Supporting Information

ABSTRACT: Plasmon-enhanced fluorescence is demonstrated in the vicinity of metal surfaces due to strong local field enhancement. Meanwhile, fluorescence quenching is observed as the spacing between fluorophore molecules and the adjacent metal is reduced below a threshold of a few nanometers. Here, we introduce a technology, placing the fluorophore molecules in plasmonic hotspots between pairs of collapsible nanofingers with tunable gap sizes at sub-nanometer precision. Optimal gap sizes with maximum plasmon enhanced fluorescence are experimentally identified for different dielectric spacer materials. The ultrastrong local field enhancement enables simultaneous detection and characterization of sharp Raman finger-prints in the fluorescence spectra. This platform thus enables in



situ monitoring of competing excitation enhancement and emission quenching processes. We systematically investigate the mechanisms behind fluorescence quenching. A quantum mechanical model is developed which explains the experimental data and will guide the future design of plasmon enhanced spectroscopy applications.

KEYWORDS: plasmonics, fluorescence, Raman spectroscopy, quantum effects, nanoimprint lithography

luorescence has many useful applications, including single molecule detection, biological labeling, and optoelectronic devices. Since the fluorescence of molecules can be strongly enhanced by increased excitation electromagnetic (EM) field intensity, plasmon-enhanced fluorescence (PEF) technology is now widely adopted, utilizing the enhancement of EM fields in the vicinity of metal nanostructures. However, while many attempts have been made in recent years to further improve the performance of PEF in applications that require high sensitivity and precision, progress has been fundamentally limited by fluorescence quenching effects in the emission process.

It has recently been demonstrated that ultrastrong EM fields can be realized between pairs of plasmonic nanostructures, which are formed by metallic nanoparticles with sub-nanometer interparticle gaps.^{6–11} Here, precise control of the physical gap at the sub-nanometer scale is critical to form strong and stable plasmonic hotspots. On the other hand, fluorescence quenching in the molecular emission process has been demonstrated at sub-5 nm scales.^{5,12} Two main factors

pose serious obstacles to understanding the mechanisms leading to fluorescence quenching experimentally. One key factor that determines fluorescence quenching is the distance between the molecule and the metal. In order to experimentally investigate the mechanism behind the continuous transition from fluorescence enhancement to fluorescence quenching, one thus needs to vary the molecule—metal distance continuously with sub-nanometer precision in the vicinity of the optimally designed plasmonic hotspots. Furthermore, since experimentally measured fluorescence intensities are simultaneously affected by the local field enhancement and fluorescence quenching mechanisms, ^{13–15}

Received: March 6, 2020 Accepted: October 21, 2020



ACS Nano www.acsnano.org Article

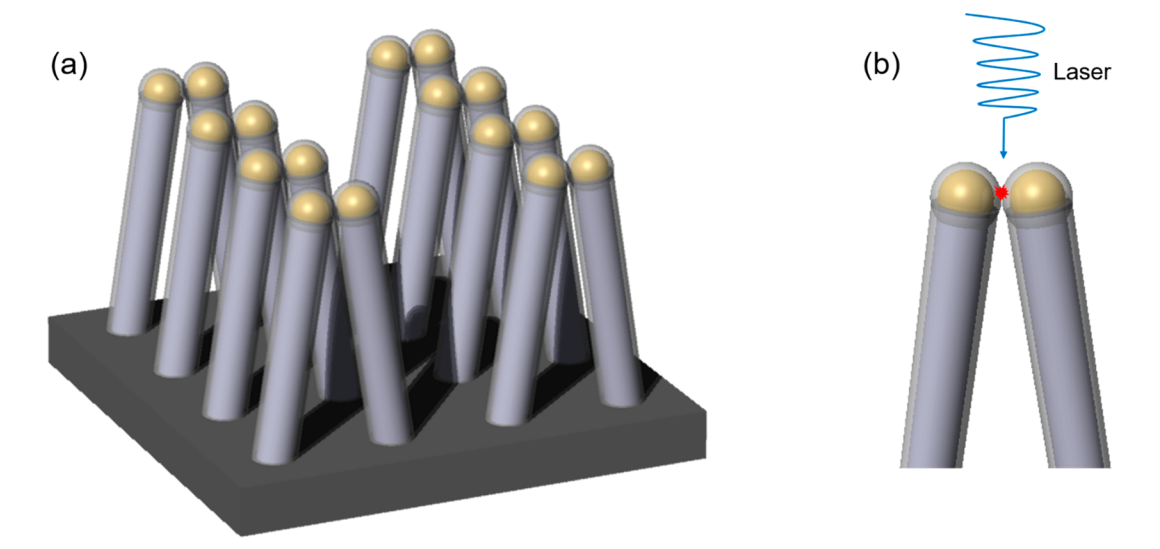


Figure 1. Schematic diagram of controllable plasmonic hot spots for fluorescence enhancement created by collapsible nanofingers. (a) Pair of metallic nanoparticles with ALD-coated dielectric layers contacting each other when flexible nanofingers beneath them collapse. The spatial gap size is defined by twice the dielectric layer thickness, and the hot spot is at the gap center. (b) Fluorescent dye molecules deposited onto collapsed nanofingers and adhere after solvent evaporation. They are then excited by the laser.

they cannot be directly used to study the contributions from both physical processes independently.

Here we present an approach to fabricate deterministically large-area gap plasmonic nanostructures with atomic precision control of gap size and molecule-metal distance, achieving high reliability and high throughput at low cost. This enables a detailed study of field enhancement and fluorescence quenching when the sub-5 nm molecule-metal distance and the gap size are varied with sub-nanometer precision. As we will discuss below, with the ultrahigh local field enhancement provided by this platform, we achieve simultaneous monitoring of fluorescence spectra with sharp Raman fingerprints inside. Since the measured Raman signal serves as an indicator of the excitation EM field, 16-18 we can use it to characterize the contribution of local field enhancement in PEF, which enables a detailed experimental study of the dominant mechanisms contributing to fluorescence quenching. This approach addresses the major challenges faced by PEF, namely, charge recombination through quantum mechanical electron tunneling at small gap sizes and nonradiative energy dissipation at small molecule-metal distances. Building on this knowledge, PEF substrates can be optimized, yielding the strongest possible plasmon enhancement with large effective area uniformly for the design of PEF based applications.

Our method is based on collapsible nanofingers fabricated using nanoimprint lithography (NIL), reactive-ion etching (RIE), and atomic-layer deposition (ALD). Figure 1a shows a schematic illustration of such gap plasmonic nanostructures. Au nanoparticles are placed on top of nanofinger pairs in flexible polymers (*i.e.*, nanoimprint resist) with high aspect ratio. A thin conformal dielectric layer is deposited uniformly by ALD onto the nanofingers before we collapse them using capillary forces. ¹⁹ The dielectric layer acts as the spacer to prevent Au nanoparticles from directly coming into contact with each other, which would induce strong electron transfer and lead to a dramatic decrease of the localized EM fields. Since the ALD process deposits the dielectric films with high conformity and atomic precision, ^{20–22} the gap size between two Au nanoparticles is accurately defined by twice the

dielectric film thickness. In order to obtain the strongest EM field enhancement at the plasmonic hotspots, the plasmonic properties can also be optimized by using different dielectric materials which impose different tunneling barrier heights for the electrons.8 When the collapsed nanofingers are used in plasmon-enhanced fluorescence, the small fluorophores are easily trapped in the saddle points of the collapsible fingers, 7,23-25 which are the regions of the hotspots at the gap center, as shown in Figure 1b. As the dielectric film covers the nanofingers uniformly, the molecule-metal distance is well-defined around the Au nanoparticles by the ALD film thickness and can be varied continuously with sub-nanometer precision. On the basis of the absorption spectra of collapsed nanofingers,8 the plasmon resonance frequency of the gap plasmonic nanostructure was determined. Next, Nile blue fluorophore was deposited onto the nanofingers, as its absorption frequency coincides with the plasmon frequency. A 633 nm wavelength laser was used to excite the Nile blue for fluorescence intensity characterization. The evolution of the Nile blue fluorescence signature peak at 667 nm was then analyzed as a function of gap size for different dielectric gap materials. We successfully identified an optimal gap size, producing the strongest fluorescence intensity enhancement uniformly over a large area. In addition, the 592 cm⁻¹ Raman fingerprint of Nile blue was examined for varying gap sizes in the corresponding fluorescence spectra. Normally, one can hardly observe fluorescence and Raman signals in the same spectra, as the Raman intensity is inherently much weaker than the fluorescence intensity. 26-28 The Raman scattering intensity, as a second order process, scales with the fourth order of the incident EM field, whereas the fluorescence intensity is proportional to the square of the EM field.^{27,29} However, the ultrastrong field enhancement obtained at the hotspots of the collapsed nanofingers facilitates the simultaneous observation of both fluorescence and Raman signals in the same spectrum. The Raman intensity is a direct in situ indicator of the localized field intensity at the plasmonic hotspots which is not affected by fluorescence quenching.³⁰ A comparison between fluorescence intensity and Raman

intensity versus dielectric gap size thus reveals the separate contributions of both field intensity and quenching mechanisms affecting the plasmon-enhanced fluorescence in the small-gap regime. As discussed below in detail, nonradiative energy dissipation and quantum tunneling both contribute at this ultrasmall scale, whereby the dielectric material determines the tunneling effect by controlling the tunneling barrier height. 11,31

RESULTS AND DISCUSSION

Figure 2a shows a scanning electron microscopy (SEM) image of 2.5 nm TiO2 coated nanofingers before the collapsing process. The fabrication procedure of collapsible nanofingers is based on nanoimprint lithography and reactive-ion etching (for details, see Methods). The nanofingers are formed by Au nanoparticles on top of UV nanoimprint resist pillars. The nanofinger arrays were fabricated uniformly over a large area (1.4 in. by 1.4 in.) with high throughput, taking advantage of NIL, 32-35 which also guarantees a good signal-to-noise ratio. It has been reported that an appropriate aspect ratio and geometry of nanofingers is critical to achieving a successful collapsing process.³⁶ The diameter and height of each nanofinger are 60 nm and 350 nm, and the pitch is 200 nm. The collapsing process is driven by capillary forces, whereby the nanofingers are soaked in ethanol and then air-dried. Similar approaches have been previously reported.^{8,19,37,3} After the collapsing process, pairs of nanofingers completely touch each other, as shown in Figure 2b. van der Waals forces keep these dimer pairs from separating once they touch.²⁵ In order to demonstrate the coverage of the TiO2 film on the Au tip of the nanofingers, a transmission electron microscopy (TEM) cross-sectional analysis of the nanogaps was performed, following the collapsing process. The TEM image in Figure 2c shows two Au nanoparticles which are separated by a 5 nm gap, i.e., twice the thickness of the ALD coated TiO₂ film. The corresponding energy-dispersive X-ray spectroscopy (EDS) maps of Au, Ti, and O shown in Figure 2d-f also confirm the 5 nm TiO2 gap between the pairs of touching Au nanoparticles. This indicates that the dielectric film covers the Au nanoparticles uniformly, acting as a spacer between the adsorbed fluorophores and the Au nanoparticles, and defining the molecule-metal distance by the dielectric film thickness. Since the precise gap size and molecule-metal distance are controlled by the ALD deposited film thickness, the varying steps can reach sub-nanometer precision. The collapsed nanofingers were then soaked in a 1 μ M Nile blue ethanol solution and air-dried for further fluorescence characterization. The dye solution was initially coated uniformly over the entire surface. Since the hotspot is a saddle area of the structure, the capillary force drove the liquid to stay around the contact points of collapsed fingers as the ethanol vaporized.^{6,7,24,25} The fluorescent Nile blue molecules were easily trapped on the bottom of the saddle area at the contact/touching point, which is the hottest plasmonic hotspot exhibiting ultrastrong EM field

The fluorescence intensity of the fluorophores is determined by two processes: (i) excitation by the incident field, which is affected by the local environment, and (ii) emission of radiation, which is influenced by the competition between radiative and nonradiative decay. Plasmon-enhanced fluorescence mainly benefits from the enhancement of the excitation process, which scales as the square of local EM field enhancement at the plasmonic hotspots. While the shrinking

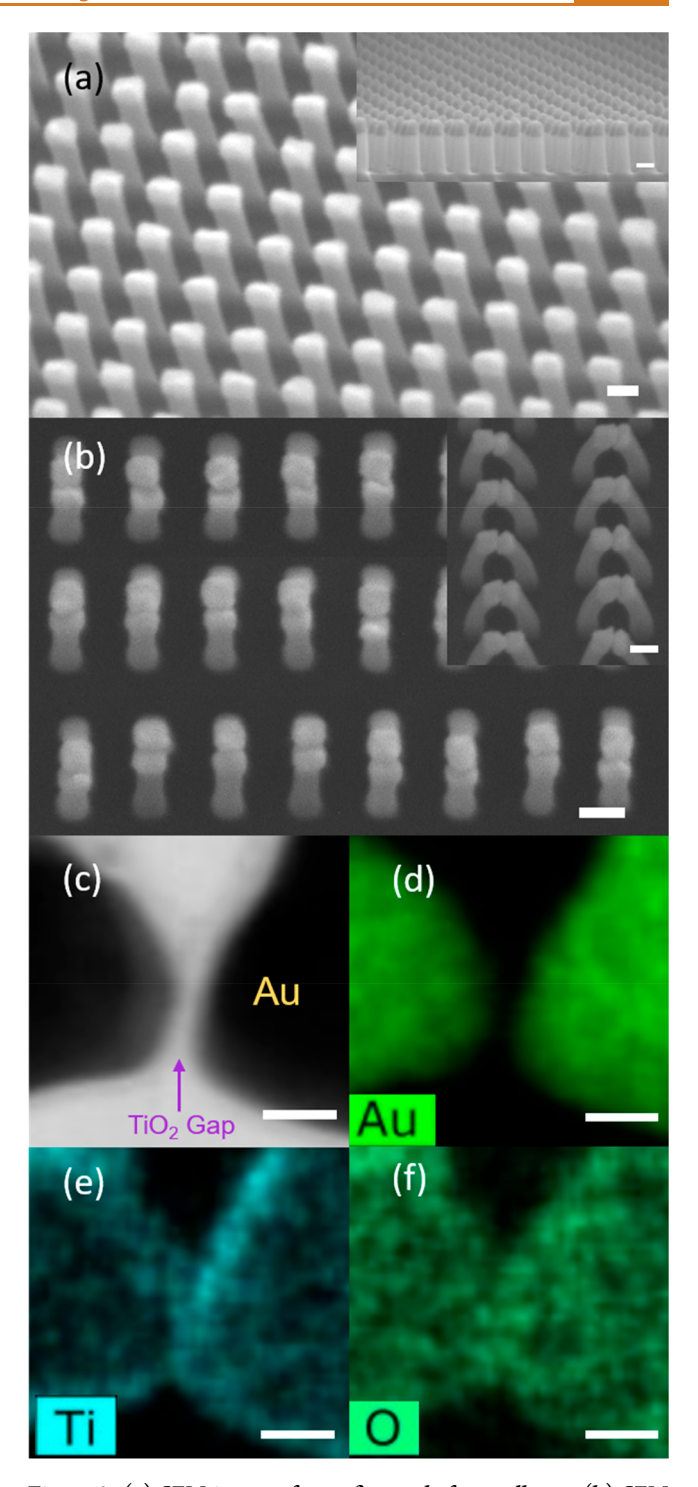


Figure 2. (a) SEM image of nanofingers before collapse. (b) SEM image of nanofingers after collapse. The inset is the image of the same nanofingers from a different viewing angle. The diameter and height of each finger are 60 nm and 350 nm. The scale bars in the SEM images are 100 nm. (c) TEM image of the dielectric nanogap inbetween the collapsed nanofingers. (d) EDS mapping of Au in the TEM image. (e) EDS mapping of Ti in the TEM image. (f) EDS mapping of O in the TEM image. The scale bars in the TEM images are 10 nm.

gap size is expected to generate increased field enhancement, fluorescence quenching also becomes significant when the gap size is reduced to the sub-5 nm regime. When the gap size is at the quantum tunneling scale, the balance between the

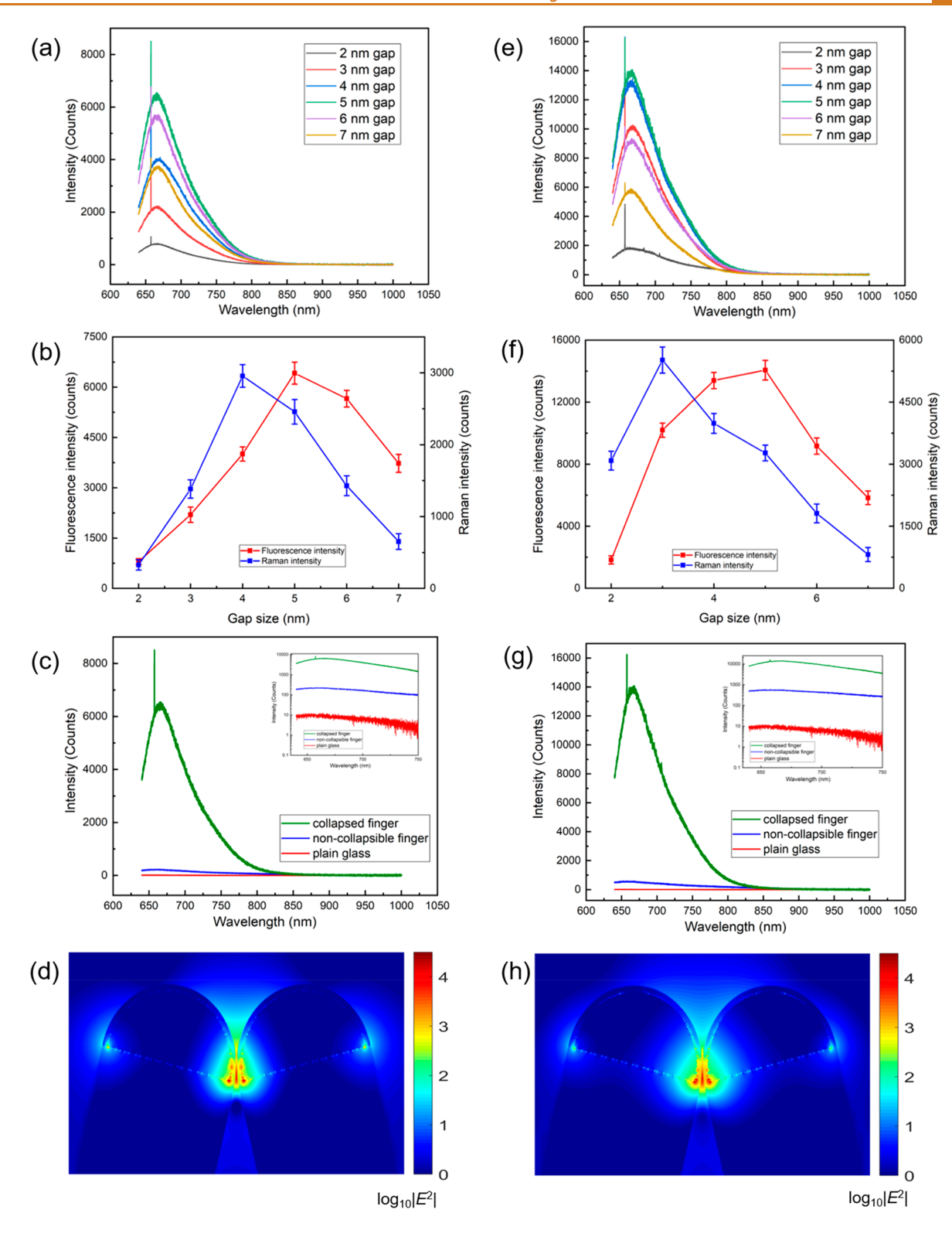


Figure 3. (a) Fluorescence intensity of Nile blue embedded between collapsed nanofingers with different TiO₂ gaps. (b) Measured fluorescence intensity and the measured 592 cm⁻¹ signature Raman intensity of Nile blue as a function of gap size. (c) Fluorescence intensity of Nile blue embedded between collapsed nanofingers with a 5 nm TiO₂ gap, compared to noncollapsible nanofingers with the same TiO₂ coating and plain glass. The inset is the corresponding logarithmic plot. (d) FDTD calculation of local field enhancement in collapsed nanofingers with a 5 nm TiO₂ gap. The corresponding plot in linear scale is also shown in Figure S1a in the Supporting Information. (e) Fluorescence intensity of Nile blue embedded between collapsed nanofingers with different Al₂O₃ gaps. (f) Measured fluorescence intensity and the measured 592 cm⁻¹ signature Raman intensity of Nile blue for different gap sizes. (g) Fluorescence intensity of Nile blue embedded between collapsed nanofingers with a 5 nm Al₂O₃ gap, noncollapsible nanofingers with the same Al₂O₃ coating, and plain glass. The inset is the corresponding logarithmic plot. (h) FDTD calculation of local field enhancement in collapsed nanofingers with a 5 nm Al₂O₃ gap. The corresponding plot in linear scale is also shown in Figure S1b in the Supporting Information.

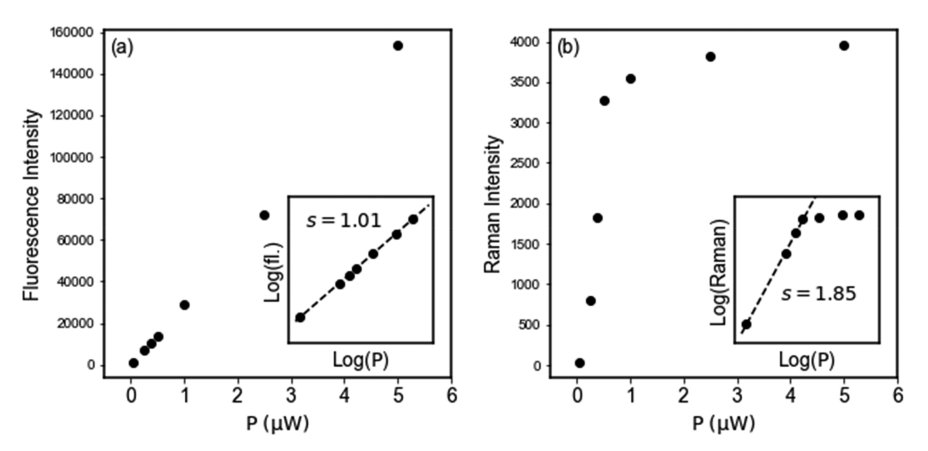


Figure 4. (a) Fluorescence intensity of Nile blue in the 5 nm Al_2O_3 gapped nanofingers subjected to different excitation powers. The inset is the corresponding logarithmic plot and the fitted slope. (b) Simultaneously measured Raman intensity of Nile blue in the 5 nm Al_2O_3 gapped nanofingers subjected to different excitation powers. The inset is the corresponding logarithmic plot and the fitted slope within a low power range.

bonding dimer plasmon and charge-transfer plasmon leads to optimal gap sizes with the maximum field enhancement, which have recently been demonstrated experimentally for different gap materials. However, the optimal gap size for field enhancement is not necessarily optimal for fluorescence enhancement. The fluorescence intensity is significantly influenced by the fluorescence quenching effect associated with Au nanoparticles, which in turn leads to a decrease of quantum yield. Charge recombination through quantum mechanical electron tunneling and nonradiative energy dissipation are strongly dependent on the molecule—metal distance and significantly decrease the fluorescence intensity in the sub-5 nm range.

In order to investigate the plasmon-enhanced fluorescence between the collapsed nanofingers, we need to reliably adjust the gap size in fine steps. Figure 3a shows the fluorescence spectra of Nile blue embedded between collapsed nanofingers with TiO₂ as the gap material. The gap sizes were chosen as 2, 3, 4, 5, 6, 7 nm, on the basis of the previously reported 4 nm optimal size for maximum EM field enhancement. 6-8 The 667 nm Nile blue fluorescence peaks (broad peaks) and the 592 cm⁻¹ Raman fingerprints (sharp peaks) were examined simultaneously for varying gap sizes. The measured fluorescence intensity and Raman intensity of Nile blue for different gap sizes are shown in Figure 3b. The fluorescence intensity reaches a maximum at 5 nm gap size, whereas the Raman intensity is at a maximum for a 4 nm gap. The gap size for strongest Raman enhancement coincides with that which exhibits the strongest plasmon light absorption, as reported before.8 However, the fluorescence intensity increases significantly when the gap is expanded from 4 to 5 nm and then gradually decreases when the gap size exceeds 5 nm. This demonstrates the competition between excitation enhancement and emission quenching processes in plasmon-enhanced fluorescence. The observed fluctuations of the fluorescence and Raman intensities originate from the measurement at different spots of large-area samples, including the influences from defects and geometry variance. The small variances of the measured intensities indicate uniform fluorescence over the entire area of large nanofinger arrays. To simulate the fluorophore excitation process, which is purely field driven, a finite-difference time-domain (FDTD) calculation of the localized EM field distribution was performed (Figure 3d).

The 633 nm plane waves polarized along the α -direction are incident from the top, perpendicular to the collapsed nanofingers with a 5 nm TiO2 gap. The settings are the same as in the experiment, which ensures the strongest plasmonic resonance and longitudinal bonding dipole plasmon mode. 43 The maximum field enhancement occurs in the vicinity of the contact point where fluorophores tend to adsorb. To evaluate the enhancement factor of PEF, the same fluorescence measurement was repeated on two control samples. One was plain glass, and the other one was made of noncollapsible nanofingers with the same dielectric coating. The noncollapsible nanofingers were fabricated similarly to the collapsible ones, but with shorter RIE etching time, which resulted in a reduced height. Hence, they did not bend and make contact during the soak-dry process. In this case, they behave essentially as a core-shell nanoparticle array, which has been widely used in previous PEF studies. 29,44 As shown in Figure 3c, the fluorescence intensity of Nile blue on the collapsed nanofingers with a 5 nm TiO₂ gap is enhanced 610fold compared to that of plain glass, whereas the enhancement factor of noncollapsible nanofingers with the same TiO2 coating is only 21-fold. Compared to strongly coupled longitudinal bonding dipole plasmon modes in the plasmonic dimers of collapsed nanofingers, the isolated core-shell monomers provide a much weaker local EM field enhancement and thus significantly reduced fluorescence intensity.

The dielectric material of the spacer has a significant influence on the plasmon-enhanced fluorescence. First, the local field at the gap is affected by the dielectric screening effect. The material with a larger dielectric constant will reduce the local electric field intensity. This will have an impact on both the excitation field enhancement and the nonradiative decay to the metal. Second, the dielectric spacer determines the quantum tunneling barrier between the Au nanoparticles which is here defined as the difference between the Fermi energy of gold (5.1 eV) and the electron affinity (EA) of the dielectric material. A higher tunneling barrier will lead to a reduced tunneling probability and therefore increased field enhancement at optimum gap size.⁴⁵ The reduced tunneling probability is manifested as a narrower optimal gap size found for the strongest field enhancement. On the basis of this field enhancement consideration, we compared the properties of Al₂O₃ and TiO₂ as gap materials between the collapsed

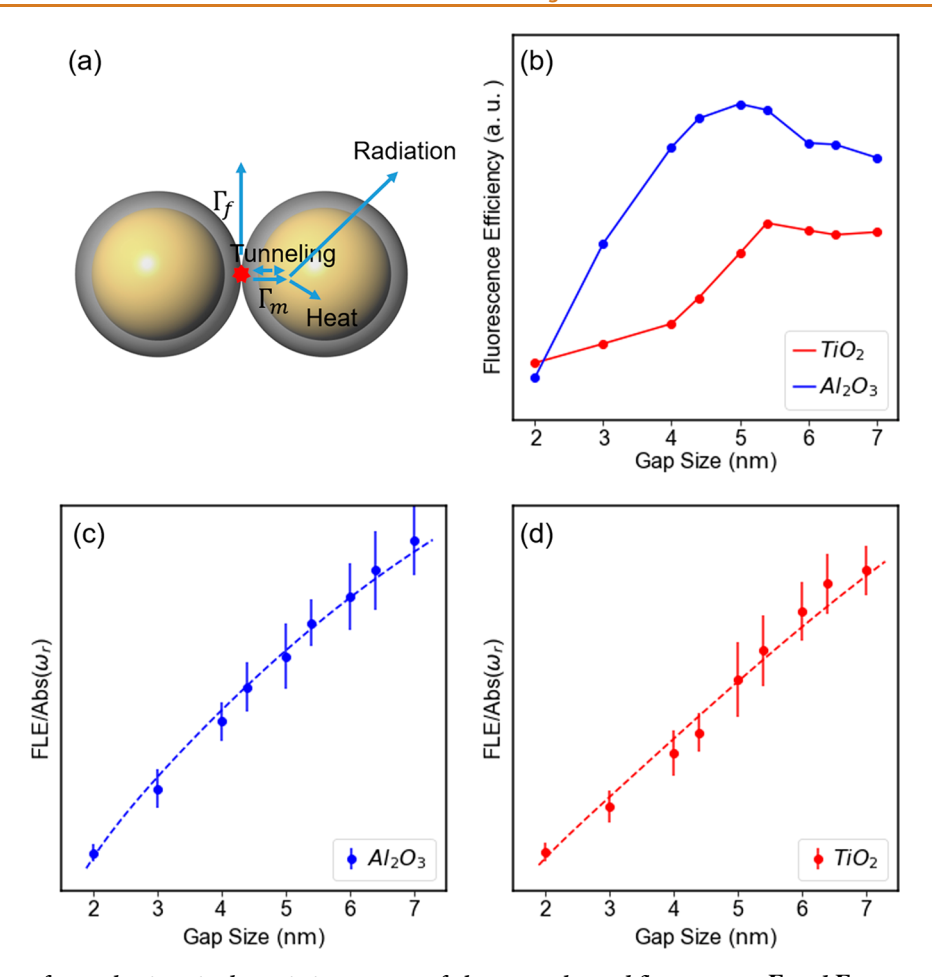


Figure 5. (a) Energy-transfer mechanisms in the emission process of plasmon-enhanced fluorescence. $\Gamma_{\rm f}$ and $\Gamma_{\rm m}$ represent the emission rates from excited molecules to free space and to adjacent Au nanoparticles; here, $\Gamma_{\rm f} \ll \Gamma_{\rm m}$. The energy transferred to Au nanoparticles can either radiate into free space or dissipate as heat. The dashed arrow represents quantum tunneling between the molecules and the Au nanoparticles. All energy-transfer channels depicted in the right Au nanosphere exist in the left Au nanosphere as well. (b) Fluorescence efficiency of Nile blue molecules embedded between collapsed nanofingers with different ${\rm TiO_2/Al_2O_3}$ gap sizes. (c) Measured ${\rm FLE/Abs}(\omega_r)$ of the molecule fluorophore for different gap sizes, with gap material ${\rm Al_2O_3}$. The data are fitted to eq 1. (d) Measured ratio ${\rm FLE/Abs}(\omega_r)$ of the molecule fluorophore for different gap sizes, with the gap material ${\rm TiO_2}$. The data are fitted to eq 1.

nanofingers. Since the electron affinities of TiO2 and Al2O3 are 4.21 and 3.71 eV, respectively, ^{46–48} Al₂O₃ retains a larger tunneling barrier height (1.39 eV) than TiO₂ (0.89 eV). We repeated the fluorescence and Raman characterization of the Al₂O₃ coated nanofingers with different gap sizes. The results are shown in Figure 3e,f. The maximal Raman intensity implies that the strongest fluorophore excitation occurs at a 3 nm Al_2O_3 gap, which is narrower than for the TiO_2 gap. However, the fluorescence intensity is weaker than that at wider gaps due to fluorescence quenching. Figure 3h shows a FDTD calculation of the localized EM field distribution in collapsed nanofingers with a 5 nm Al₂O₃ gap. The fluorescence enhancement of the 5 nm Al₂O₃ gapped nanofingers enhance the Nile blue fluorescence 1526-fold, uniformly across the large area, which is larger than the largest fluorescence enhancement in TiO₂ gapped nanofingers (Figure 3g). This can be attributed to the reduction of electron tunneling and nonradiative energy dissipation from molecule to metal in the emission process, as the Al₂O₃ spacer provides a higher tunneling barrier and a stronger screening for the radiation field than TiO2, which ultimately leads to an increased quantum efficiency and overall fluorescence intensity. We also measure the fluorescence and Raman signals of Nile blue in the 5 nm Al₂O₃ gapped nanofingers subjected to different excitation powers, which are shown in Figure 4. It is interesting to see that they show very different variations with the power change. The fluorescence signal scales as E^2 for a large range of the excitation power, whereas the Raman signal only scales as E^4 at low powers and then saturates at higher powers. This phenomenon has not been reported before, but it is an important guide for us to choose proper excitation power levels for the investigation of the fluorescence quenching mechanism using the simultaneously measured Raman intensity.

To gain a deeper understanding of the fluorescence quenching phenomena observed in our experiment, here we provide an analytical model to describe the emission process of the excited fluorophores, which can ultimately guide the effective design of potential applications. There have been extensive studies of fluorescence quenching phenomena in gap plasmonic structures with relatively large molecule—metal separations and variation steps where the pure classical electromagnetic theory is usually applied. 5,12,49,50 However, the mechanisms of fluorescence quenching become more complicated when the gap sizes shrink to the quantum mechanical scale due to the participation of the quantum tunneling effect. Here we consider the effects from both the

nonradiative energy dissipation and the quantum electron tunneling in the plasmon-enhanced fluorescence. To analyze the fluorescence quenching mechanisms which contribute to the emission process, we first eliminate the field enhancement effect that contributes to the fluorescence intensity in the fluorophore molecule excitation process. Since the simultaneously measured Raman intensity is a direct indicator of the localized field intensity at low excitation power levels, which is not affected by the fluorescence quenching, we divide the fluorescence intensity by the square root of the simultaneously measured Raman intensity and define the ratio as the fluorescence efficiency (FLE) which purely depicts the emission process contributing to the fluorescence intensity. Figure 5b shows the FLE of Nile blue embedded between the collapsed nanofingers with two gap materials, TiO₂ and Al₂O₃, for different values of the gap size d. Here we address the three dominant physical processes involved in the variation of the FLE with d, which are sketched in Figure 5a. First, the excited Nile blue molecules radiate to the Au-nanoparticle dimers with an emission rate $\Gamma_{\rm m}$, which can be derived using the Weisskopf–Wigner approach. Since the molecules are surrounded by Au nanoparticles, direct radiation from the molecules into free space, Γ_{θ} is negligible.³⁰ It turns out that $\Gamma_{\rm m}$ depends on the electromagnetic local density of states (LDOS) $\rho(\omega_r)$ at the emission frequency ω_r (=667 nm) of the molecule. This LDOS, which in turn depends on the geometric structure of the dimer cavity, describes the number of available photon modes in the dimer cavity at the emission frequency of Nile blue and furthermore determines the energy-transfer strength from the fluorescent molecules to the Au nanoparticles. Here we use the experimentally measured net absorption spectrum of the Au-nanoparticle dimer cavity to obtain this energy-transfer efficiency. The absorption spectra of the sample before the nanofingers collapsed were measured and deducted from the final results after collapse. The background absorption due to the metal and dielectric material is therefore canceled out, and the net spectrum can properly reflect the characteristics of the local cavity formed by the gapped dimer structure. The net absorption at the frequency $\omega_{\rm r}$, labeled as Abs($\omega_{\rm r}$), is recorded for different gap sizes. Second, the energy emitted to the Au nanoparticles can either radiate into free space (to be detected as the fluorescence signal) or dissipate as heat (Ohmic loss).³⁰ Since the radiation wavelength is much larger than the distance between molecules and the surface of Au nanoparticles, by using the electrostatic approximation and the image-charge method,⁵³ we find that the Ohmic loss is proportional to $1/d^4$ (see Figure S2 in the Supporting Information). Furthermore, at such a small gap distance, electron tunneling between the molecules and the Au nanoparticles leads to a weakening of the radiative fluorophore dipole $p_r \rightarrow p_r(1 - e^{-\lambda d/2})$, where $e^{-\lambda d/2}$ accounts for the tunneling probability.⁸ Noticing that Ohmic loss and tunneling effects are more significant for smaller gap sizes, we arrive at a phenomenological formula for fluorescence efficiency,

FLE =
$$A \cdot Abs(\omega_r) \left(1 - \frac{B}{d^4}\right) (1 - e^{-\lambda d/2})^2$$
 (1)

From here we can see that the FLE is determined by the energy emitted from the molecules to the Au nanoparticles (\sim Abs($\omega_{\rm r}$)), subject to tunneling and Ohmic loss. We experimentally obtain the ratio $\frac{{\rm FLE}}{{\rm Abs}(\omega_{\rm r})}$ and then fit it to the

function $A\left(1-\frac{B}{d^4}\right)(1-\mathrm{e}^{-\lambda d/2})^2$ for the two gap materials, as shown in Figure 5c,d. Triple standard deviation was applied as the error to the fitting for a confidence interval of 99.7%, which indicates a permissible error range. The inverse of the fitting parameter λ measures the characteristic tunneling length of the gap material. By fitting the experimental data, we find that $1/\lambda_{\mathrm{TiO}_2}\approx 3.11\pm 0.27$ nm and $1/\lambda_{\mathrm{Al_2O_3}}\approx 2.34\pm 0.12$ nm, indicating that TiO_2 has a larger characteristic length of tunneling than $\mathrm{Al_2O_3}$. This qualitatively agrees with the fact that TiO_2 has a smaller tunneling barrier than $\mathrm{Al_2O_3}$. Simple estimation 54 from our fitting parameters indicate that the tunneling barrier of $\mathrm{Al_2O_3}$ is about $\left(\frac{\lambda_{\mathrm{Al_2O_3}}}{\lambda_{\mathrm{TiO_2}}}\right)^2\approx 1.77$ times higher than that for TiO_2 , which is close to the known electron tunneling barrier ratio $\frac{1.39\ \mathrm{eV}}{0.89\ \mathrm{eV}}\approx 1.56$. The parameter B measures the strength of nonradiative decay. We find $B_{\mathrm{TiO_2}}\approx 5.94\pm 0.44$ and $B_{\mathrm{Al_2O_3}}\approx 8.29\pm 0.75$, which qualitatively agrees with the fact that $\mathrm{Al_2O_3}$ has a smaller dielectric constant than $\mathrm{TiO_2}$. The quantum tunneling term introduced in our

measures the strength of nonradiative decay. We find $B_{\text{TiO}} \approx$ 5.94 ± 0.44 and $B_{Al_2O_3} \approx 8.29 \pm 0.75$, which qualitatively agrees with the fact that Al₂O₃ has a smaller dielectric constant than TiO2. The quantum tunneling term introduced in our model naturally makes the fitting much better than a fitting without including this (see Figure S3 in the Supporting Information). We observe that the tunneling and Ohmic losses to the metallic nanoparticles decrease as the gap size is increased. On the other hand, a close match between the inherent emission frequency of fluorophore molecules and the strong absorption frequency of the gap plasmonic structure is beneficial to increase the fluorescence intensity. We should mention that this model only holds for small gap sizes (<10 nm), as the coupling between the fluorophore molecules and metallic nanoparticles decays with increased distances. Since the strongest field enhancement and therefore excitation remain within this small gap range, this model will be useful for the design of applications with high precision and intensity requirements.

CONCLUSIONS

In summary, we have demonstrated a technology to experimentally investigate plasmon-enhanced fluorescence at the sub-nanometer scale, where strong fluorescence quenching occurs. We have experimentally identified optimal gap sizes for maximum plasmon-enhanced fluorescence with tunable dielectric spacers. This technology enables us to position fluorophore molecules in the hottest region of gap plasmonic hotspots, resulting in ultrastrong field enhancement. Using this approach, we have simultaneously observed fluorescence and the Raman signal in the same spectra, which enables the interpretation and analytical modeling of the leading fluorescence quenching mechanism at small gap sizes. This platform provides an opportunity to analyze plasmonenhanced fluorescence with in situ monitoring of the local field enhancement, which enables the exclusion of the field enhancement contribution, thus isolating the quantum mechanical quenching mechanism. These results provide the guidance for future design of plasmon-enhanced applications, such as chemical sensing and biological labeling which require ultrahigh sensitivity and accuracy.

METHODS

Nanofinger Sample Preparation. The two-dimensional grid mother molds were prepared by self-developed interference

lithography. The nanofinger samples were fabricated on 1.4 in. square plain glass substrates, on the basis of the combination of nanoimprint lithography (EZImprinting Inc.) and reactive-ion etching (Oxford PlasmaPro 100). Following the NIL and RIE processes, the Au nanoparticles were deposited *via* e-beam evaporation (Temescal BJD-1800 E-Beam Evaporator) at 10° off-normal incidence, which created asymmetric shaped Au nanoparticles and facilitated collapse in a dimer geometry. The following lift-off and deep RIE process created high aspect ratio collapsible nanofingers on the underlying thick UV nanoimprint resist (I-UVP, 15% concentration; EZImprinting). The dielectric spacers with different thicknesses were deposited *via* atomiclayer deposition (Ultratech Simply ALD). Au coated flat monitor samples were used during the ALD deposition process for the accurate monitoring of ALD film thickness by ellipsometry (VASE ellipsometer).

SEM, TEM, and EDS Measurements. SEM images were taken by JEOL JSM 7001 operated at 8 kV accelerating voltage with an averaging working distance at 8.5 mm. Samples for TEM (JEOL, JEM 2100F) cross-section characterization at the gap were prepared by a dual beam FIB (Seiko 4050MS) parallel to the dimer direction.

Fluorescence and Raman Spectroscopies. Fluorescence and Raman spectra characterizations of fluorophore molecules were performed by a Renishaw inVia Raman microscope. The pumping laser used was 633 nm and kept at $0.5~\mu W$. A $50\times$ standard objective lens was used to focus excitation light at the measuring spot. The incident light polarization was along the dimer direction. Nile blue (Sigma-Aldrich) powder was dissolved in analytical ethanol (Sigma-Aldrich) with $1~\mu M$ concentration. A 0.1~mL aliquot of Nile blue solution was coated uniformly over the entire sample surface (1.4 in. by 1.4 in.) and dried in air. On average, an estimate of 5 molecules were trapped in each hot spot with $100~mm^2$ surface area.

ASSOCIATED CONTENT

Supporting Information

The Supporting Information is available free of charge at https://pubs.acs.org/doi/10.1021/acsnano.0c01973.

Electric field distribution plotted in a linear scale; calculation of electromagnetic energy loss to the surface of Au nanoparticles; fitting the fluorescence efficiency without including the quantum tunneling effect (PDF)

AUTHOR INFORMATION

Corresponding Author

Wei Wu − Ming Hsieh Department of Electrical Engineering, University of Southern California, Los Angeles, California 90089, United States; oorcid.org/0000-0001-6404-0317; Email: wu.w@usc.edu

Authors

Boxiang Song — Ming Hsieh Department of Electrical Engineering, University of Southern California, Los Angeles, California 90089, United States; orcid.org/0000-0002-4946-2738

Zhihao Jiang — Department of Physics and Astronomy, University of Southern California, Los Angeles, California 90089, United States

Zerui Liu – Ming Hsieh Department of Electrical Engineering, University of Southern California, Los Angeles, California 90089, United States

Yunxiang Wang — Ming Hsieh Department of Electrical Engineering, University of Southern California, Los Angeles, California 90089, United States

Fanxin Liu — Department of Applied Physics, Zhejiang University of Technology, Hangzhou, Zhejiang, China 310023 Stephen B. Cronin — Ming Hsieh Department of Electrical

Engineering, University of Southern California, Los Angeles,

California 90089, United States; o orcid.org/0000-0001-9153-7687

Hao Yang — Ming Hsieh Department of Electrical Engineering, University of Southern California, Los Angeles, California 90089, United States; Oorcid.org/0000-0002-0992-9161

Deming Meng – Ming Hsieh Department of Electrical Engineering, University of Southern California, Los Angeles, California 90089, United States

Buyun Chen – Ming Hsieh Department of Electrical Engineering, University of Southern California, Los Angeles, California 90089, United States

Pan Hu – Ming Hsieh Department of Electrical Engineering, University of Southern California, Los Angeles, California 90089, United States

Adam M. Schwartzberg — Molecular Foundry, Lawrence Berkeley National Laboratory, Berkeley, California 94720, United States; Oorcid.org/0000-0001-6335-0719

Stefano Cabrini — Molecular Foundry, Lawrence Berkeley National Laboratory, Berkeley, California 94720, United States

Stephan Haas – Department of Physics and Astronomy, University of Southern California, Los Angeles, California 90089, United States

Complete contact information is available at: https://pubs.acs.org/10.1021/acsnano.0c01973

Author Contributions

[⊥]B.S. and Z.J. contributed equally to this work.

Notes

The authors declare no competing financial interest.

ACKNOWLEDGMENTS

We thank Dr. A. F. Levi for helpful discussion. W.W. acknowledges support from the National Science Foundation (NSF) Grant No. CMMI-1635612. S.H. acknowledges support from the Department of Energy under Grant No. DE-FG02-05ER46240. S.B.C. acknowledges support from NSF Award No. CHE-1708581. F.L. acknowledges support from the National Natural Science Foundation of China under Grant Nos. 11574270 and 11974015. Work at the Molecular Foundry was supported by the Office of Science, Office of Basic Energy Sciences, of the U.S. Department of Energy under Contract No. DE-AC02-05CH11231.

REFERENCES

- (1) Kinkhabwala, A.; Yu, Z.; Fan, S.; Avlasevich, Y.; Müllen, K.; Moerner, W. E. Large Single-Molecule Fluorescence Enhancements Produced by a Bowtie Nanoantenna. *Nat. Photonics* **2009**, *3*, 654–657.
- (2) Bauch, M.; Toma, K.; Toma, M.; Zhang, Q.; Dostalek, J. Plasmon-Enhanced Fluorescence Biosensors: A Review. *Plasmonics* **2014**, *9*, 781–799.
- (3) Heo, M.; Cho, H.; Jung, J.-W.; Jeong, J.-R.; Park, S.; Kim, J. Y. High-Performance Organic Optoelectronic Devices Enhanced by Surface Plasmon Resonance. *Adv. Mater.* **2011**, *23*, 5689–5693.
- (4) Tam, F.; Goodrich, G. P.; Johnson, B. R.; Halas, N. J. Plasmonic Enhancement of Molecular Fluorescence. *Nano Lett.* **2007**, *7*, 496–501.
- (5) Anger, P.; Bharadwaj, P.; Novotny, L. Enhancement and Quenching of Single-Molecule Fluorescence. *Phys. Rev. Lett.* **2006**, *96*, 113002.
- (6) Hu, J.; Yu, H.; Su, G.; Song, B.; Wang, J.; Wu, Z.; Zhan, P.; Liu, F.; Wu, W.; Wang, Z. Dual-Electromagnetic Field Enhancements through Suspended Metal/Dielectric/Metal Nanostructures and

- Plastic Phthalates Detection in Child Urine. Adv. Opt. Mater. 2020, 8, 1901305.
- (7) Liu, F.; Song, B.; Su, G.; Liang, O.; Zhan, P.; Wang, H.; Wu, W.; Xie, Y.; Wang, Z. Sculpting Extreme Electromagnetic Field Enhancement in Free Space for Molecule Sensing. *Small* **2018**, *14*, 1801146.
- (8) Song, B.; Yao, Y.; Groenewald, R. E.; Wang, Y.; Liu, H.; Wang, Y.; Li, Y.; Liu, F.; Cronin, S. B.; Schwartzberg, A. M.; et al. Probing Gap Plasmons Down to Subnanometer Scales Using Collapsible Nanofingers. ACS Nano 2017, 11, 5836—5843.
- (9) Schuller, J. A.; Barnard, E. S.; Cai, W.; Jun, Y. C.; White, J. S.; Brongersma, M. L. Plasmonics for Extreme Light Concentration and Manipulation. *Nat. Mater.* **2010**, *9*, 193–204.
- (10) Halas, N. J.; Lal, S.; Chang, W.-S.; Link, S.; Nordlander, P. Plasmons in Strongly Coupled Metallic Nanostructures. *Chem. Rev.* **2011**, *111*, 3913–3961.
- (11) Marinica, D. C.; Kazansky, A. K.; Nordlander, P.; Aizpurua, J.; Borisov, A. G. Quantum Plasmonics: Nonlinear Effects in the Field Enhancement of a Plasmonic Nanoparticle Dimer. *Nano Lett.* **2012**, *12*, 1333–1339.
- (12) Dulkeith, E.; Morteani, A.; Niedereichholz, T.; Klar, T.; Feldmann, J.; Levi, S.; Van Veggel, F.; Reinhoudt, D.; Möller, M.; Gittins, D. Fluorescence Quenching of Dye Molecules near Gold Nanoparticles: Radiative and Nonradiative Effects. *Phys. Rev. Lett.* **2002**, *89*, 203002.
- (13) Akselrod, G. M.; Argyropoulos, C.; Hoang, T. B.; Ciracì, C.; Fang, C.; Huang, J.; Smith, D. R.; Mikkelsen, M. H. Probing the Mechanisms of Large Purcell Enhancement in Plasmonic Nanoantennas. *Nat. Photonics* **2014**, *8*, 835.
- (14) Baumberg, J. J.; Aizpurua, J.; Mikkelsen, M. H.; Smith, D. R. Extreme Nanophotonics from Ultrathin Metallic Gaps. *Nat. Mater.* **2019**, *18*, 668–678.
- (15) Rose, A.; Hoang, T. B.; McGuire, F.; Mock, J. J.; Ciracì, C.; Smith, D. R.; Mikkelsen, M. H. Control of Radiative Processes Using Tunable Plasmonic Nanopatch Antennas. *Nano Lett.* **2014**, *14*, 4797–4802.
- (16) McCall, S.; Platzman, P.; Wolff, P. Surface Enhanced Raman Scattering. *Phys. Lett. A* **1980**, *77*, 381–383.
- (17) Krug, J. T.; Wang, G. D.; Emory, S. R.; Nie, S. Efficient Raman Enhancement and Intermittent Light Emission Observed in Single Gold Nanocrystals. *J. Am. Chem. Soc.* 1999, 121, 9208–9214.
- (18) Stiles, P. L.; Dieringer, J. A.; Shah, N. C.; Van Duyne, R. P. Surface-Enhanced Raman Spectroscopy. *Annu. Rev. Anal. Chem.* **2008**, *1*, 601–626.
- (19) Duan, H.; Berggren, K. K. Directed Self-Assembly at the 10 Nm Scale by Using Capillary Force-Induced Nanocohesion. *Nano Lett.* **2010**, *10*, 3710–3716.
- (20) George, S. M. Atomic Layer Deposition: An Overview. *Chem. Rev.* **2010**, *110*, 111–131.
- (21) Elam, J.; Routkevitch, D.; Mardilovich, P.; George, S. Conformal Coating on Ultrahigh-Aspect-Ratio Nanopores of Anodic Alumina by Atomic Layer Deposition. *Chem. Mater.* **2003**, *15*, 3507–3517.
- (22) Standridge, S. D.; Schatz, G. C.; Hupp, J. T. Toward Plasmonic Solar Cells: Protection of Silver Nanoparticles *via* Atomic Layer Deposition of TiO₂. *Langmuir* **2009**, *25*, 2596–2600.
- (23) Kim, A.; Ou, F. S.; Ohlberg, D. A. A.; Hu, M.; Williams, R. S.; Li, Z. Study of Molecular Trapping inside Gold Nanofinger Arrays on Surface-Enhanced Raman Substrates. *J. Am. Chem. Soc.* **2011**, *133*, 8234–8239.
- (24) Hu, M.; Ou, F. S.; Wu, W.; Naumov, I.; Li, X.; Bratkovsky, A. M.; Williams, R. S.; Li, Z. Gold Nanofingers for Molecule Trapping and Detection. *J. Am. Chem. Soc.* **2010**, *132*, 12820–12822.
- (25) Ou, F. S.; Hu, M.; Naumov, I.; Kim, A.; Wu, W.; Bratkovsky, A. M.; Li, X.; Williams, R. S.; Li, Z. Hot-Spot Engineering in Polygonal Nanofinger Assemblies for Surface Enhanced Raman Spectroscopy. *Nano Lett.* **2011**, *11*, 2538–2542.
- (26) Hartschuh, A.; Pedrosa, H. N.; Novotny, L.; Krauss, T. D. Simultaneous Fluorescence and Raman Scattering from Single Carbon Nanotubes. *Science* **2003**, *301*, 1354–1356.

- (27) Li, J.-F.; Li, C.-Y.; Aroca, R. F. Plasmon-Enhanced Fluorescence Spectroscopy. *Chem. Soc. Rev.* **2017**, *46*, 3962–3979.
- (28) Cadusch, P.; Hlaing, M.; Wade, S.; McArthur, S.; Stoddart, P. Improved Methods for Fluorescence Background Subtraction from Raman Spectra. *J. Raman Spectrosc.* **2013**, *44*, 1587–1595.
- (29) Guerrero, A. R.; Zhang, Y.; Aroca, R. F. Experimental Confirmation of Local Field Enhancement Determining Far-Field Measurements with Shell-Isolated Silver Nanoparticles. *Small* **2012**, *8*, 2964–2967.
- (30) Pelton, M. Modified Spontaneous Emission in Nanophotonic Structures. *Nat. Photonics* **2015**, *9*, 427.
- (31) Teperik, T. V.; Nordlander, P.; Aizpurua, J.; Borisov, A. G. Quantum Effects and Nonlocality in Strongly Coupled Plasmonic Nanowire Dimers. *Opt. Express* **2013**, *21*, 27306–27325.
- (32) Yao, Y.; Liu, H.; Wang, Y.; Li, Y.; Song, B.; Bratkovsk, A.; Wang, S.-Y.; Wu, W. Nanoimprint Lithography: An Enabling Technology for Nanophotonics. *Appl. Phys. A: Mater. Sci. Process.* **2015**, 121, 327–333.
- (33) Gates, B. D.; Xu, Q.; Stewart, M.; Ryan, D.; Willson, C. G.; Whitesides, G. M. New Approaches to Nanofabrication: Molding, Printing, and Other Techniques. *Chem. Rev.* **2005**, *105*, 1171–1196.
- (34) Chou, S. Y.; Krauss, P. R.; Renstrom, P. J. Nanoimprint Lithography. J. Vac. Sci. Technol., B: Microelectron. Process. Phenom. 1996, 14, 4129–4133.
- (35) Zhang, M.; Pacheco-Peña, V.; Yu, Y.; Chen, W.; Greybush, N. J.; Stein, A.; Engheta, N.; Murray, C. B.; Kagan, C. R. Nanoimprinted Chiral Plasmonic Substrates with Three-Dimensional Nanostructures. *Nano Lett.* **2018**, *18*, 7389–7394.
- (36) Chandra, D.; Yang, S. Capillary-Force-Induced Clustering of Micropillar Arrays: Is It Caused by Isolated Capillary Bridges or by the Lateral Capillary Meniscus Interaction Force? *Langmuir* **2009**, *25*, 10430–10434.
- (37) Kotera, M.; Ochiai, N. Three-Dimensional Simulation of Resist Pattern Deformation by Surface Tension at the Drying Process. *Microelectron. Eng.* **2005**, *78*, 515–520.
- (38) Chini, S. F.; Amirfazli, A. Understanding Pattern Collapse in Photolithography Process Due to Capillary Forces. *Langmuir* **2010**, 26, 13707–13714.
- (39) Alivisatos, A.; Arndt, M.; Efrima, S.; Waldeck, D.; Harris, C. Electronic Energy Transfer at Semiconductor Interfaces. I. Energy Transfer from Two-Dimensional Molecular Films to Si (111). *J. Chem. Phys.* **1987**, *86*, 6540–6549.
- (40) Aslan, K.; Lakowicz, J. R.; Szmacinski, H.; Geddes, C. D. Metal-Enhanced Fluorescence Solution-Based Sensing Platform. *J. Fluoresc.* **2004**, *14*, 677–679.
- (41) Aslan, K.; Malyn, S. N.; Geddes, C. D. Metal-Enhanced Fluorescence from Gold Surfaces: Angular Dependent Emission. *J. Fluoresc.* **2006**, *17*, 7–13.
- (42) Albella, P.; Moreno, F.; Saiz, J.; González, F. Surface Inspection by Monitoring Spectral Shifts of Localized Plasmon Resonances. *Opt. Express* **2008**, *16*, 12872–12879.
- (43) Yang, L.; Wang, H.; Fang, Y.; Li, Z. Polarization State of Light Scattered from Quantum Plasmonic Dimer Antennas. *ACS Nano* **2016**, *10*, 1580–1588.
- (44) Li, J. F.; Huang, Y. F.; Ding, Y.; Yang, Z. L.; Li, S. B.; Zhou, X. S.; Fan, F. R.; Zhang, W.; Zhou, Z. Y.; Wu, D. Y.; et al. Shell-Isolated Nanoparticle-Enhanced Raman Spectroscopy. *Nature* **2010**, 464, 392–395.
- (45) Tan, S. F.; Wu, L.; Yang, J. K.; Bai, P.; Bosman, M.; Nijhuis, C. A. Quantum Plasmon Resonances Controlled by Molecular Tunnel Junctions. *Science* **2014**, *343*, 1496–1499.
- (46) Wu, H.; Wang, L. S. Electronic Structure of Titanium Oxide Clusters: TiO_y (y = 1 3) and $(TiO_2)_n$ (n = 1 4). *J. Chem. Phys.* 1997, 107, 8221–8228.
- (47) Archibong, E. F.; St-Amant, A. On the Structure of Al_2O_3 and Photoelectron Spectra of Al_2O_2 and Al_2O_3 . *J. Phys. Chem. A* **1999**, 103, 1109–1114.
- (48) Desai, S. R.; Wu, H.; Rohlfing, C. M.; Wang, L.-S. A Study of the Structure and Bonding of Small Aluminum Oxide Clusters by

ACS Nano www.acsnano.org Article

- Photoelectron Spectroscopy: $Al_xO_y-(x=1-2, y=1-5)$. *J. Chem. Phys.* **1997**, 106, 1309–1317.
- (49) Habenicht, B. F.; Prezhdo, O. V. Nonradiative Quenching of Fluorescence in a Semiconducting Carbon Nanotube: A Time-Domain *ab Initio* Study. *Phys. Rev. Lett.* **2008**, *100*, 197402.
- (50) Gaudreau, L.; Tielrooij, K.; Prawiroatmodjo, G.; Osmond, J.; de Abajo, F. G.; Koppens, F. Universal Distance-Scaling of Nonradiative Energy Transfer to Graphene. *Nano Lett.* **2013**, *13*, 2030–2035.
- (51) Weisskopf, V.; Wigner, E. P. Calculation of the Natural Brightness of Spectral Lines on the Basis of Dirac's Theory. *Eur. Phys. J. A* **1930**, *63*, 54–73.
- (52) Scully, M. O.; Zubairy, M. S. *Quantum Optics*, 1st ed.; Cambridge University Press: Cambridge, U.K., 1997; Vol. 1, pp 291–300
- (53) Jackson, J. D. Classical Electrodynamics, 3rd ed.; John Wiley & Sons: New York, NY, USA, 1998; Vol. 1, pp 145–169.
- (54) Ling, S. J.; Sanny, J.; Moebs, W. *University Physics*, 1st ed.; Physics LibreTexts: Davis, CA, USA, 2016; Vol. 3, pp 278–285.